NJC

Accepted Manuscript

PAPER

Monitoring by *in situ* neutron diffraction of simultaneous dehydration and Ni²⁺ mobility in partially exchanged NaY zeolite†

Florence Porcher,[a,b] Jean-Louis Paillaud,[c] Lucia Gaberova,[d] Gilles André,[a] Sandra Casale,[d,e] Pascale Massiani[d,e*]

Powder neutron diffraction is used to follow structural changes occurring during heat and vacuum assisted dehydration of 3wt% nickel exchanged NaY. The structures determined from Rietveld refinement confirm the nickel ions displacement from the supercages and sodalite cages towards hexagonal prisms upon water removal. Not only this mobility but also its relationship with dehydration level is demonstrated, owing to real time quantification of dehydration through changes of the intensity of the incoherent neutron scattering signal. Comparison with TGA data proves that this signal is fully attributable to water molecules adsorbed in the zeolite. STEM/EDX and *in situ* heating TEM studies provide complementary information on homogeneous Ni distribution (initial state) and on reductive sintering in vacuum at high temperature.

1. Introduction

In the large family of aluminosilicates, zeolites have unique behaviours provided by their peculiar structural and chemical properties. Their structures consist of crystalline TO_2 frameworks constituted of tetrahedral T (Si or Al) atoms bridged by oxygen atoms, in such way as to delimit organized networks of pores with high surface area and diameters (often between 5 and 10 Å) close to those of many molecules. These steric features are the keystone of the well-know applications of zeolites as molecular sieves or adsorbents[1] as well as in fields such as selective gas separation[2] or shape selective catalysis.[3]

The other specificity of zeolites lies in the tetrahedral aluminum atoms inserted as trivalent Al^{3+} in their TO_2 network that generate framework negative charges (one per framework Al atom). For the sake of neutrality, these charges are neutralized by charge compensating cations (alkali, protons, metal ions...) located in their proximity, in the pores. Global chemical formula of zeolites may be written as $A_x^{a+}B_y^{b+}C_z^{c+}...(H_2O)_m[Si_{1-n}Al_nO_2]$, where x+ y + z (etc.) = n and A, B, C (etc.) are compensating cations of distinct natures with respective valences a, b, c (etc.).

The easy exchange of these cations by others, especially in solution, makes zeolites highly performing as cationic exchangers, for instance in laundry or water purification domains. This cationic exchange propensity also allows the easy tuning of their chemical composition, as often required in heterogeneous catalysis when dispersion of metal active sites (cations or nanoparticles) on porous supports is targeted.[4,5] In such case, not only the metal content but also the metal location, the metal-framework interactions or the distribution between co-cations, if present, can play a determining role. Understanding these features therefore often represent a prerequisite for good control of material properties. This has prompted the numerous studies on cationic sites identification in zeolites since the pioneering works of Breck and Flanigen[6] and of Barrer[7] on synthetic zeolites. The propensity of cations to move from one site to another eventually positioned far away upon adsorption of a molecule (water, reactants...) has been also well demonstrated[8] and widely studied, notably in the case of transition metal exchanged zeolites for DeNOx catalysis.[9-11]

Amongst works dedicated to the description of cations in zeolites, many have been focussed on faujasite with structural topology FAU[12] that is one of the most studied zeolites. As reviewed in the late 90's[13] and schematized on Fig. 1, five main types of cationic sites (called I, I', II, II' and III) were defined in this structure to facilitate the comparison of alkali distributions in samples with various cations and different hydration states.[14] These sites are also currently considered for transition metal cations, even if small local shifts often need to be taken into account, particularly for multivalent ions such as Ni^{2+} exchanged in faujasites with varying basicities.[15,16]

a. *Laboratoire Léon Brillouin (LLB), UMR 12 CNRS-CEA, 91191 Gif-sur-Yvette Cédex, France.*
b. *Université de Lorraine, UMR 7036 CNRS, CRM2, Faculté des Sciences et Technologies, BP 70239, Boulevard des Aiguillettes, 54506 Vandoeuvre-lès-Nancy, France.*
c. *Equipe Matériaux à Porosité Contrôlée (MPC), Institut de Science des Matériaux de Mulhouse (IS2M), UMR CNRS 7361, Université Haute-Alsace, 3bis rue Alfred Werner, 68093 Mulhouse Cedex, France*
d. *Sorbonne Université - Université Paris 06 UPMC, Laboratoire de Réactivité de Surface (LRS), 4 place jussieu, 75005 Paris cédex, France*
e. *CNRS UMR 7197, LRS - UPMC, 4 place jussieu, 75005 Paris cédex, France. E-mail: pascale.massiai@upmc.fr*
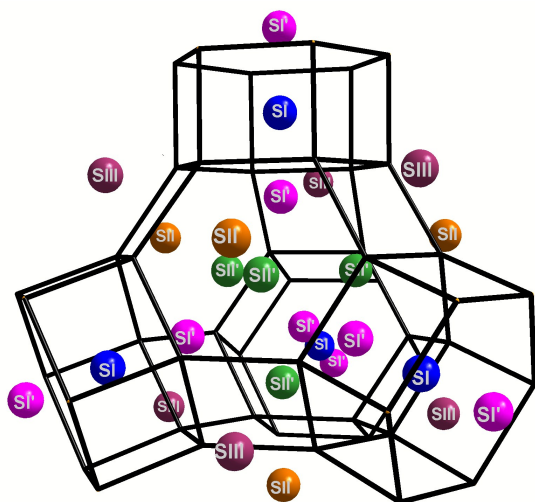
Fig. 1: Schematic representation of the cubic faujasite (FAU) structure with location of cationic sites I, I', II, II' and III. Site I is located at the centre of the hexagonal prism, I' and II' inside the sodalite cage and II and III in the supercage. For reasons of clarity, framework oxygen atoms have been omitted.

In recent works, theoretical ab initio (DFT) calculations were often used to get precise description of the sites and of the interactions of cations with the framework.[11,15] Nevertheless, for computing capacity reasons, the models have to be restricted to small clusters representing only a small portion of the zeolite unit cell. Consequently, they are not adapted to the study of cations displacements between sites eventually positioned far away from each other. Monte Carlo approaches (less precise but considering a larger zone) can then help, and be adapted to systems containing heavy elements (e.g. metal ions) as well, especially in presence of a restricted number of water molecules, provided that appropriate force fields have been previously established.[17,18] Therefore, description of the cation mobility still relies greatly on experiments.

Considering the peculiar case of Ni^{2+}, the first attempt to locate it in Ni-NaFAU was done by XRD in the 70's.[19] The effect of temperature was next analysed by various techniques including XRD,[20] EPR[21] or XAS.[22] From these works, it is commonly admitted that in the hydrated sample nickel is located at site II, inside the supercage that is big enough (pore diameters of the order of 13 Å)[12] to accommodate the water hexa-coordinated Ni^{2+} cluster; above 573 K (dehydrated state), Ni^{2+} tends on the contrary to move to sites I (centre of the hexagonal prism or *d6r*) where it can optimize its coordination by interacting with the framework oxygen atoms.[15,23,24] Nevertheless, none of above cited techniques allows following "*in real time*" the dehydration process. Especially, with XRD, water content is estimated only after structural refinement and a very crude knowledge on water content is usually obtained: most often, one has then to perform additional *ex situ* additional experiments (such as TG), which is not best suited for establishing properly a correlation between two processes (presently water removal and structural changes). Moreover, a drawback of XRD for the study of limited Ni^{2+}

amounts in zeolites is the low contrast for this element compared to Na^+ that lie on the same sites. Besides, techniques such as XAS or EPR give an average picture without discriminating between sites positions.

In addition to above techniques, neutron diffraction has been also widely used to characterize zeolite structures and cationic sites occupancies. Commonly, the works are carried out after careful sample dehydration[25-32] or after deuteration[33-39] in order to avoid the known neutron scattering by hydrogen that decreases data quality and renders interpretations more complex. Nevertheless, we will show in the present contribution that this effect, in place of being a drawback, can on the contrary be very fruitfully exploited to characterise simultaneously water removal and nickel mobility in zeolites. Neutron diffraction is moreover highly sensitive to nickel, which exhibits a large scattering length of 10.3 fm[40], which makes it particularly appropriate for the study of Ni containing zeolites.

To conduct the work, we selected a partially nickel-exchanged NaY (FAU structure, Si/Al=2.3) for two main reasons. Firstly, the well-established knowledge on cationic sites positions in FAU[13,14] can significantly help identifying Ni^{2+} displacements upon dehydration. Secondly, the FAU structure contains three distinct types of cages (supercages, sodalites and hexagonal prisms) that facilitate the experimental observation of mobility from one cage to another. We therefore applied this technique to monitor in situ and "*in real time*" conditions the water removal occurring together with structural evolutions along evacuated heating treatment. The nickel amount in the sample was kept low (≈3 wt %) to ensure that its atomic content is below the number of available hexagonal prisms.

2. Experimental

2.1 Sample preparation

The parent NaY sample was a synthetic Linde SK-40 zeolite from Union Carbide Corporation with framework Si/Al ratio of 2.3. This sample was exchanged with Ni by classical exchange method in solution. The latter consisted in stirring at room temperature for 24 h a suspension made of 100 mL of 4 mM $Ni(NO_3)_2$ aqueous solution (containing ≅ 23 mg Ni) and of 1 g of parent hydrated zeolite (i.e. > 720 mg of dehydrated zeolite, see TGA data below). The sample was washed three times in distilled water, recovered by centrifugation (green powder) and dried overnight at 350 K in a static oven (pink powder). It was finally let to fully rehydrate at room temperature and atmosphere for one month before analysis. Note that a rapid colour change from pink to green (both typical of Ni^{2+}, bare and hydrated respectively) attested easy rehydration.

2.2 Neutron Diffraction

The neutron powder diffraction patterns were recorded on the high-flux, cold neutrons powder diffractometer G4-1 and on the high resolution, thermal neutron powder diffractometer 3T2 of the LLB-Orphée facility at CEA/Saclay (for partially-hydrated/dehydrated and hydrated samples, respectively). G4-

1 is equipped with a vertically focusing 200 pyrolytic graphite monochromator (nominal wavelength of 2.4226 Å) and a 800-cells multi-detector covering a 80° range in 2θ (Δθ = 0.1° between 2 cells). An evacuated heating chamber allowed registering the evolution of the diffractograms versus temperature (range 293-873 K). To this end, the sample (about 300 mg) was placed in an open vanadium sample holder in a furnace under vacuum (P~10⁻⁵ mbar). A first diffraction pattern was recorded at room temperature (RT) not longer after pumping was started (hydrated sample) then temperature was progressively increased while continuously recording the pattern (2θ between 8 and 88°, 15 min per scan). Finally, the sample was cooled down to room temperature and a last pattern was taken (dehydrated sample). The hydrated (evacuated) sample was also analysed on the 3T2 diffractometer whose larger resolution range allows ful refinement of the structural parameters (atomic positions, occupancies, displacement parameters) while G4.1 is focused on fast data acquisition and thermodiffractometry. Rietveld refinements[41] were performed with the FullProf Suite.[42]

2.3 Complementary techniques

Chemical composition was obtained from elemental analysis measured by dispersive X-ray fluorescence spectroscopy using a PHILIPS MagiX apparatus. Thermogravimetric analysis (TGA) was carried out on a STD Q600 thermobalance (TA Instrument) using 20 mg of zeolite powder. After 15 min stabilisation at room temperature in flowing air (20 mL.min⁻¹), the weight loss was followed while regularly increasing the temperature up to 873 K (7 K.min⁻¹). Electron microscopy studies were performed on a LaB6 transmission electron microscope JEOL JEM2010 operating at 200kV. STEM EDX mappings were acquired to visualise the Ni dispersion in the zeolite support and X-Ray characteristics of the following elements were recorded: K-O, K-Al, K-Si, K-Na and K-Ni (PGT detector). Other TEM experiments were made using a single tilt "Heating sample Holder" (EM-SHH4, Gatan) that allowed *in situ* heating of the sample up to 873 K while simultaneously observing selected zones. The micrographs were registered on an ORIUS Gatan Camera. In both modes, the sample powder was suspended in hexane (for better dispersion) before observation then deposited on a 3 mm grid of copper (STEM EDX observations) or Mo (heating experiments) covered with an ultrathin carbon membrane of around 10 nm thickness.

3. Results and discussion

3.1 Homogeneous Ni dispersion in the hydrated sample

The unit cell composition of the as-prepared hydrated exchanged zeolite was $(Ni^{2+})_7(Na^+)_{31}(H^+)_{13}[Al_{58}Si_{134}O_{384}](H_2O)_{270}$ (where H_2O is present as adsorbed molecule in the pores). In reference to its unit cell Ni atomic content, the sample will be hereafter named Ni₇NaY. This composition confirms firstly that part of the sodium cations (58 Na per unit cell in the parent zeolite) were exchanged by nickel ones, as expected after treatment in the nickel nitrate solution. Secondly, the atomic nickel content

(about 7 Ni per unit cell) corresponds to c.a. 3.1 wt% Ni (with respect to the dehydrated sample), only slightly below the nickel content in the exchange suspension. This illustrates the propensity of Ni^{2+} ions to replace Na^+ ones in zeolites. Thirdly, the atomic content per unit cell (7 Ni^{2+} and 31 Na^+) is slightly lower than expected for charge neutrality, suggesting presence of some protons, possibly introduced as well by exchange process, in line with the slightly acidic pH of the suspension (around 5). Fourthly, the number of nickel atoms per unit cell (7) is about half that of double prisms per unit cell (16), which ensures that all nickel ions have the possibility to move upon dehydration to confined sites I (expected preferred location).

Before diffraction studies, combined STEM and EDX mappings were performed to check the good nickel distribution all over the sample. Representative images are shown in Fig. 2. On the STEM picture (image on top left), Ni₇NaY crystals appear as truncated octahedra about 1 μm in size. STEM-EDX mappings on the same zone reveal a highly homogenous distribution of all elements (Si, Al, Na, Ni, O), including nickel (in green). For sodium, however, initial low brightness was obtained (due to combination of the rather low molecular weight of this element, making it less sensitive, and to its content) and contrast had therefore to be reinforced, explaining the lower quality of the image. Nevertheless, it is confirmed that nickel exchange took place and led to a very good nickel repartition in all zeolite grains.
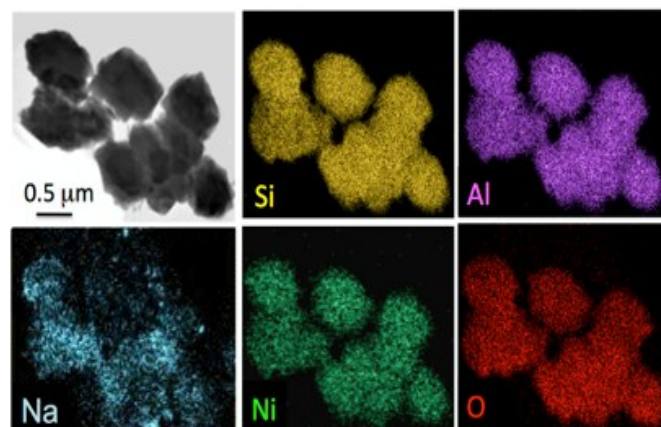

Fig. 2. STEM image of the exchanged Ni₇NaY sample and silicon (yellow), aluminum (purple), sodium (blue), nickel (green), and oxygen (red) EDX mappings.

3.2 Quantification of dehydration from Neutron Diffraction patterns

The structural evolution of the Ni₇NaY sample during heating in vacuum up to 873 K was next studied by powder neutron diffraction. The diffractograms recorded along treatment in the 8< 2θ < 88° range are shown in Fig. 3A. Whatever the temperature, the diffraction patterns are typical of the FAU structure, without additional peak detected, attesting of the crystalline purity of the sample.

As classically observed for zeolites, changes in peak intensities versus temperature were also noted. This is illustrated in Fig. 3B for the most intense Bragg peak, 111.[43] The evolution of intensity for this peak is also quantified in Fig. 4a. The slight shift towards larger angles when temperature increases, also

visible on Figure 3B and similarly present (not shown) for other peaks, reveals the well known negative thermal expansion of faujasite-type zeolite upon heating and after water removal.[44] More interestingly, a regular - and simultaneous - decrease of the baseline level is seen, and this is even better visualized in Fig. 3C and in the 3D waterfall plot representation shown in Fig. 3D (restricted to the 2θ range between 13° and 48° for the sake of clarity). This signal is due to the extremely large incoherent cross section of ^1H atoms[45] attributable mainly to water molecules filling the pores as proposed in our recent work on $Na_{58}Y$[18] and in an earlier study on gypsum dehydration.[46]

To confirm the origin of the neutron scattering signal and validate its relationship with hydration level, we compared the evolution of this signal intensity versus temperature (Fig. 4b) with the weight loss plot obtained by thermo-gravimetric analysis in flowing air (Fig. 4c). Even if both plots are not perfectly superimposed (possibly due to different treatment conditions, namely in vacuum and in air, respectively), their trends are very close, confirming above attribution.

Therefore, in addition to give access to structural properties, neutron diffraction informs "*in real time*" on water removal, and the process can be easily quantified. In spite of the strong interest of such simultaneous observation, neutron diffraction was to our knowledge scarcely exploited as such in the past, except for the above-cited work on kinetics of dehydration of gypsum.[46]
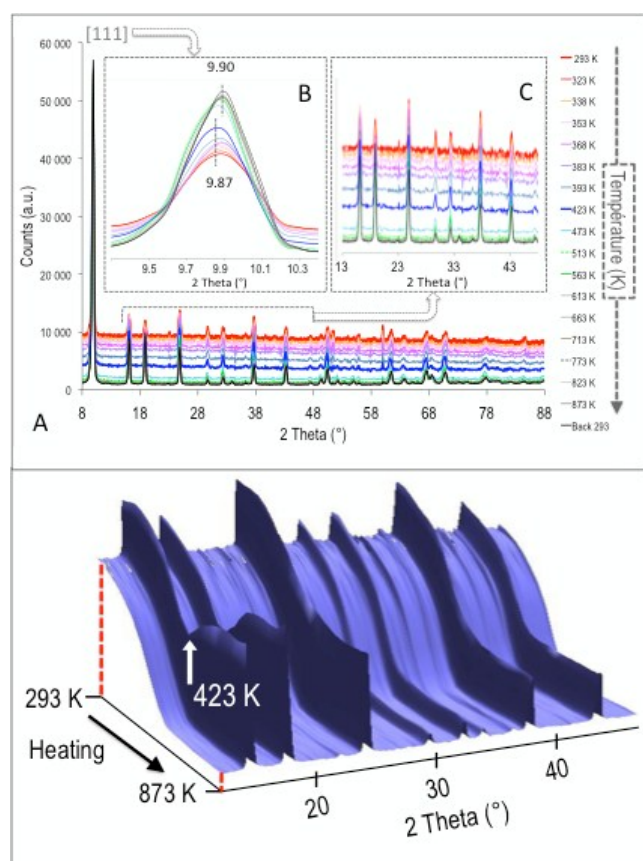

Fig. 4: Evolution versus temperature (from 293K up to 773 K, then cooling back to RT) of the (a) intensity of the 111 neutron diffraction peak (2θ at c.a. around 9.9°) and (b) level of incoherent signal; (c) comparison with weight loss (red plain line) measured by TG in air flow.

From curve b in Fig. 4, it can also be seen that dehydration is rather regular between 293 K (RT) and c.a. 473 K, afterwards the process significantly slows down. Therefore, a significant amount of water (around 40%) is still present after the boiling point of liquid water (373 K) has been reached, and some molecules remain adsorbed till a temperature as high as 573 K. This confirms the strong interactions of water with the zeolite adsorbent. Finally full dehydration seems to take place at about 573 K (as detected more precisely with neutron diffraction than with TGA) and the weight loss estimated from TGA after full dehydration is 28wt% *i.e.*, about 270 water molecules per unit cell. Note, however, that this value is probably slightly below the real value for fully hydrated Ni_7NaY because the sample was let to stabilize at RT in flowing gas for 5 min in the TGA instrument before heating was started. Therefore, some previous - even if limited - dehydration can have occurred during this step, and the same situation holds for neutron diffraction experiments since the first pattern was taken after the sample was evacuated at RT.

3.3 Nickel displacement and related structural changes with water removal

The structural characteristics of the Ni_7NaY sample along heating were next determined from Rietveld refinement. For the 3T2 datasets, an unconstrained refinement of atomic positions was possible, thanks to the large resolution range of the diffractometer. For the G4.1 thermodiffractograms restraints on T-O distances (T-O = 1.66 ±0.01 Å) were introduced in order to limit the number of refined parameters. Atomic displacement parameters were kept fixed to standard values in all cases. Extra framework atoms were fully refined including occupancy factors.

Two examples of refinement are shown in Fig. 5A (423 K) and Fig. 5B (623 K). Both reveal the data quality and the good agreement between measurement and simulation. The inset in Fig. 5C illustrates, once again, and for these two temperatures, the drastic change in baseline intensity level already discussed in the previous paragraph.

Fig. 3: Powder neutron diffraction patterns of Ni_7NaY during heating from 293 to 873 K: (A) general evolution and zooms on (B) the 111 peak and (C) background level (18-48° 2q range); (D) waterfall plot representation between 13° and 48° highlighting the regular decrease of incoherent signal intensity (dotted red lines) and the quasi-total dehydration step at 423 K (white arrow).
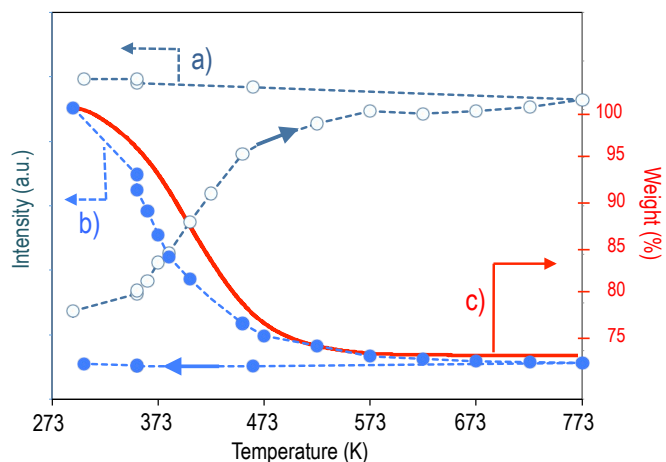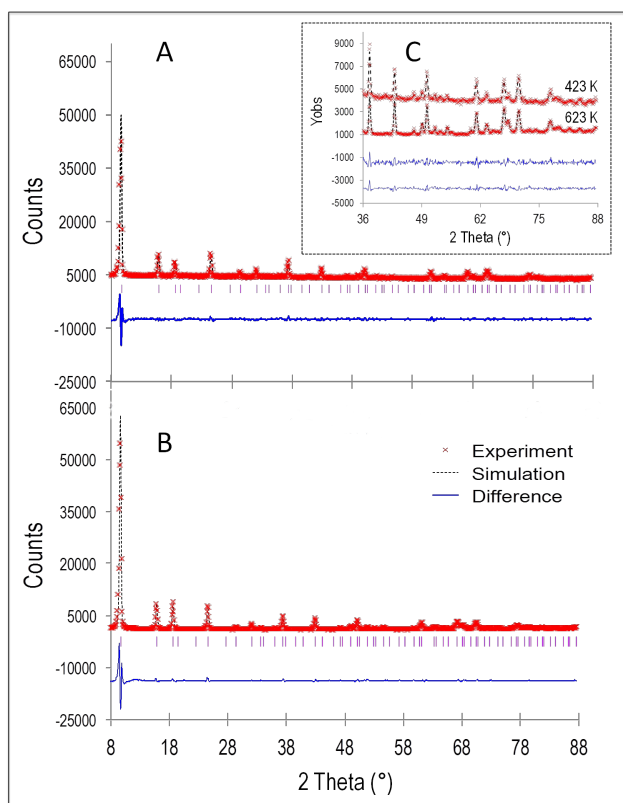
Fig. 5: Rietveld refinements of neutron diffraction patterns of Ni₇NaY heated in vacuum at (A) 423 K and (B) 623K: experimental (red crosses), simulated (dotted black lines) and difference (plain blue lines) data. (C) Zoom comparing the different levels of incoherent signal at these two temperatures.

From these refinements, atomic coordinates in the zeolitic framework and at extra-framework positions (cations and adsorbed water molecules) were obtained. Table 1 reports the data for 4 representative distinct steps of dehydration, namely 293 K (hydrated sample, data from 3T2), 423 K, 623 K and back to RT (dehydrated sample) (data from G4.1). The corresponding structures are schematized in Fig. 6 and the evolutions of sites occupancies for all covered temperatures are shown in Fig. 7. For reasons that will be detailed in the next section, the experiment for the fully dehydrated sample had to be repeated by heating the sample at a maximum temperature of 573 K, then cooling it back to RT. The results in Table 1 and in Fig. 6 are those of this second measurement.

From these series of data, several conclusions can be drawn. Firstly, the cations occupancies (Table 1) and structures found for hydrated and dehydrated Ni₇NaY (Figures 6A and 6D, respectively) confirm the already reported propensity of Ni²⁺ (i) to be localized at site I' in the sodalite cages and to a less extend at site II in the hydrated (evacuated) sample[13] and (ii) to move towards the centre of hexagonal prisms (site I) after water removal (to find higher confinement). For the limited nickel content presently studied, this last location is definitively the only one occupied by nickel after dehydration. Surprisingly, all the Na⁺ ions were found to be located in the sodalite cage at site II' in the hydrated form (Fig. 7), which is not commonly observed. However, Na⁺ ions position at site II and II' in a Y faujasite of composition (Ni₂₁Na₁₇Al₅₉Si₁₃₃O₃₈₄)

partially dehydrated under air was previously reported.[47] This is in fact not very far from the recording conditions applied on 3T2 since the analysis chamber was evacuated at the beginning of the experiment (to remove atmospheric water). The small amount of protons in our sample may also play a role. Unfortunately, the lack of very precise data between room temperature and 423 K, precludes to determine if the transfer of the Na⁺ ions from sodalite cages (site II') in the hydrated form towards site II upon dehydration (Fig. 7) is a progressive or abrupt phenomenon. Secondly, intermediate steps are seen above 423 K, with preferential Ni²⁺ location in sites I' at 423 K, then in sites I when reaching 623 K (Table 1 and Fig. 6 and 7). Interestingly, it appears that nickel displacement from site I' towards sodalite cages starts only around 423 K, after more than 70% of the water molecules have been removed (Fig. 4b), and the displacement from sites I' (in sodalite cages, at the entrance of hexagonal prisms) to sites I (inside the hexagonal prisms) occurring between 523 K and 623 K (Fig. 7) is associated to the removal of the last 10% water molecules (Fig. 4b).
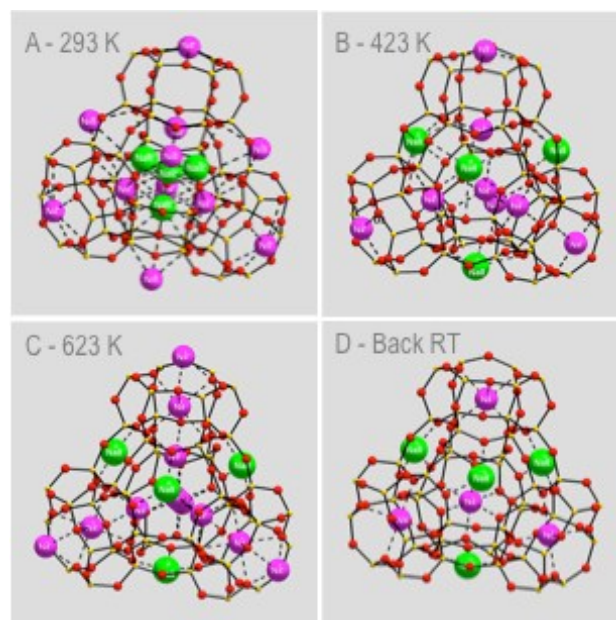

Fig. 6: Experimental structures showing main cations locations as deduced from Rietveld analysis of Ni7NaY heated in vacuum at 293 K (hydrated sample), 473 K, 573 K and after dehydration (back to RT). The framework O atoms (red balls), the tetrahedral Si or Al (yellow balls), the Na⁺ cations (green balls) and the Ni²⁺ cations (magenta balls) are represented. For the sake of clarity, water molecules are not shown.

From this discussion, it appears that a strong interest of neutron diffraction is to allow correlating the structural changes and cations migrations to specific - and quantified - dehydration levels. Nevertheless, it has to be recalled that the present experiments were performed in dynamic conditions, while heating. This can bring some uncertainty on the identification of temperatures at which peculiar steps occur, compared to experiments involving temperature stabilisation steps, as will be presented in a next paper (to be published). In this next paper, the framework distortions occurring upon water removal and the determining role of water rather than temperature towards such distortions will be discussed.

Table 1: Examples of coordinates and sites occupancies for framework atoms, cations and adsorbed water molecules in Ni$_7$NaY after heating in vacuum at different temperatures (space group *Fd3m*).

	Atom	Wyck.[a]	S.O.F.[b]	x/a	y/b	z/c	U [Å²][c]
3T2 : 293 K (hydrated) (a = 24.7116(5) Å, R$_f$ = -1.0 %)	O1	96h	1	-0.1063(4)	0	0.1063(4)	0.0266
	O2	96g	1	0.2516(4)	0.2516(4)	0.1417(5)	0.0266
	O3	96g	1	0.1738(4)	0.1738(4)	0.1417(5)	0.0266
	O4	96g	1	0.1766(4)	0.1766(4)	0.3265(6)	0.0266
	Si	192i	0.6979	0.1256(4)	-0.0546(4)	0.0350(5)	0.0122
	Al	192i	0.3021	0.1256(4)	-0.0546(4)	0.0350(5)	0.0122
	Na(II')	32e	0.784(6)	0.170(1)	0.170(1)	0.170(1)	0.0380
	Ni (I')	32e	0.111(5)	0.057(5)	0.057(5)	0.057(5)	0.0380
	Ni (II)	32e	0.08(2)	0.270(4)	0.270(4)	0.270(4)	0.0380
	O (w1)	32e	0.20(4)	0.305(3)	0.305(3)	0.305(3)	0.0380
	O (w2)	32e	0.26(9)	0.072(3)	0.072(3)	0.072(3)	0.0380
G4.1 : 423 K (a=24.765(2) Å, R$_f$ = 3.4 %)	O1	96h	1	-0.1066(6)	0	0.1066(6)	0.0266
	O2	96g	1	0.2500(11)	0.2500(11)	0.1442(14)	0.0266
	O3	96g	1	0.1730(12)	0.1730(12)	-0.0359(12)	0.0266
	O4	96g	1	0.1793(11)	0.1793(11)	0.3259(12)	0.0266
	Si	192i	0.6979	0.1267(3)	-0.0538(3)	0.0359(4)	0.0122
	Al	192i	0.3021	0.1267(3)	-0.0538(3)	0.0359(4)	0.0122
	Ni (I')	32e	0.181(4)	0.054(5)	0.054(5)	0.054(5)	0.0380
	Na (II)	32e	0.45(14)	0.242(7)	0.242(7)	0.242(7)	0.0380
	O (w1)	32e	0.217(6)	0.298(7)	0.298(7)	0.298(7)	0.0380
G4.1 : 623 K (a=24.758(2) Å, R$_f$ = 8.1 %)	O1	96h	1	-0.1082(5)	0	0.1082(5)	0.0266
	O2	96g	1	0.2539(9)	0.2539(9)	0.1428(10)	0.0266
	O3	96g	1	0.1815(7)	0.1815(7)	-0.0306(9)	0.0266
	O4	96g	1	0.1744(9)	0.1744(9)	0.3147(12)	0.0266
	Si	192i	0.6979	0.1220(3)	-0.0535(3)	0.0357(4)	0.0122
	Al	192i	0.3021	0.1220(3)	-0.0535(3)	0.0357(4)	0.0122
	Ni (I')	32e	0.039(3)	0.071(16)	0.071(16)	0.071(16)	0.0380
	Na (II)	32e	0.911(11)	0.233(3)	0.233(3)	0.233(3)	0.0380
	Ni (I)	16c	0.356(5)	1/4	0	1/4	0.0380
G4.1 : Back RT (dehydrated) (a = 24.725(2) Å, R$_f$ = 8.2 %)	O1	96h	1	-0.1086(5)	0	0.1086(5)	0.0266
	O2	96g	1	0.2537(8)	0.2537(8)	0.1437(10)	0.0266
	O3	96g	1	0.1840(7)	0.1840(7)	-0.0321(9)	0.0266
	O4	96g	1	0.1729(9)	0.1729(9)	0.3153(11)	0.0266
	Si	192i	0.6979	0.1218(3)	-0.0534(3)	0.0356(4)	0.0122
	Al	192i	0.3021	0.1218(3)	-0.0534(3)	0.0356(4)	0.0122
	Ni (I')	8a	0.009(3)	0.07(7)	0.07(7)	0.07(7)	0.0380
	Na (II)	32e	1	0.232(2)	0.232(2)	0.232(2)	0.0380
	Ni (I)	16c	0.428(5)	1/4	0	1/4	0.0380

[a] Multiplicity and Wyckoff letter
[b] Site occupancy factors
[c] Temperatures factors were fixed to an average value for (Si, Al) = T, O framework atoms and extra-framework species.
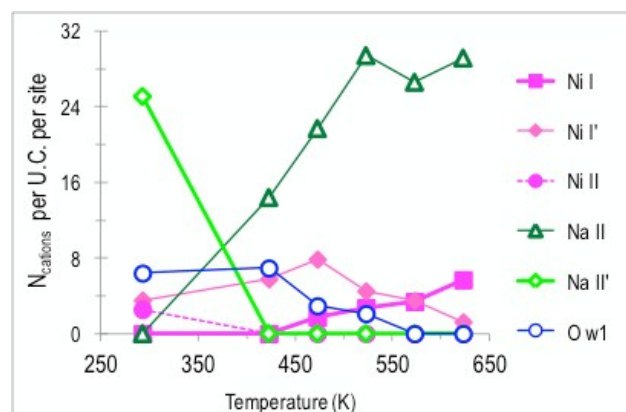

Fig. 7: Evolution with temperature (293-623 K range) of the number of Ni^{2+} and Na$^+$ cations, and of water molecules (Ow1) per unit cell in each type of cationic site (I, I', II, II').

3.4 Complementary *In situ* heating TEM experiments

Finally, complementary TEM experiments were carried out, for the following reason. It is often advised to perform zeolite dehydration both in vacuum and at high temperatures to ensure full water removal. Such conditions were respected in the present neutron experiments. Nevertheless, after the first experiment in which the sample was heated up to 873 K, we observed a slight colour change of the sample that turned grey. TEM observations were therefore performed: they revealed the presence, after heating, of small nanoparticles.

To analyse further this evolution, a dedicated TEM study was conducted using a heating sample holder. This allowed following the evolution of given zones of the Ni$_7$NaY sample during *in situ* heating in the microscope, in vacuum (as for the neutron diffraction experiments). An example is shown on Fig. 8. The image registered for the hydrated sample shows a small regular truncated octahedral crystal with no additional phase detected (Fig. 8a). At higher magnification, the high crystallinity and the regular porous system are very well identified (Fig. 8a') confirming the structural quality of the sample after exchange already stressed out in § 3.1. At 573 K, however, small black spots start to be visible, suggesting some nickel reduction (Fig. 8b and zoom in 8b') and the process is strongly accentuated when temperature increases up to 873 K, nanoparticles 5-15 nm in size being then distinguished all over the zeolite grain (Fig. 8c and zoom in 8c'). Even if the sensitivity of metal cations to reduction upon heating in vacuum is rather well known, the present work stresses the fact that great care should be taken to avoid such process if heat and vacuum assisted dehydration of zeolites containing transition metal ions is targeted.
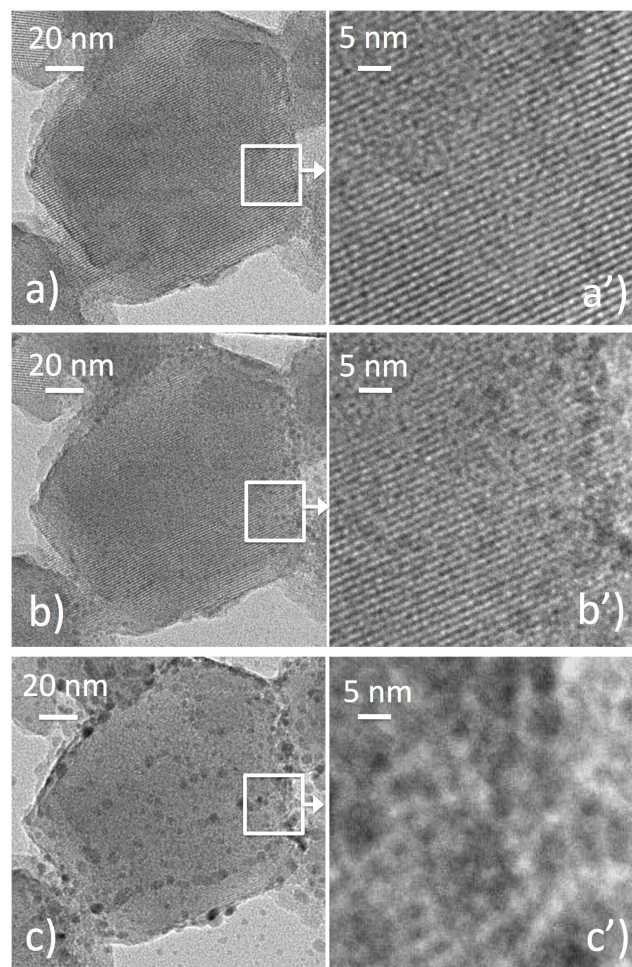

Fig. 8: Evolution of transmission electron micrographs of a same Ni$_7$NaY crystal during in situ heating on the heating sample holder in vacuum, in the microscope chamber: micrographs registered at (a) 293 K, (b) 573 K and (c) 873 K and (a', b', c') zooms on the zones (white rectangles) shown on the main pictures.

New Journal of Chemistry Accepted Manuscript

4. Conclusions

Neutron diffraction is shown to be a very powerful technique for the study of zeolites dehydration and establishment of correlations between water removal and cations mobility. By comparison with XRD that is commonly used to determine structural properties, neutron diffraction has the strong advantage, if water content is concerned, to allow water quantification together with structures determination. Moreover, the information can be very easily obtained during the experiment thanks to the intensity of the ^{1}H incoherent signal that is related to water content and can be estimated directly from the diffraction pattern, *in real time*. Unambiguous relationship between hydration level and cationic sites occupancies can thus be obtained. Moreover, the high sensitivity of neutron scattering in this respect allows detecting low amounts of remaining adsorbed water at temperatures as high as 473 K, with a precision that is higher than with TG experiments. Full dehydration in Ni-NaY is reached around 573 K, a temperature that should in fact not be exceeded in vacuum conditions, since reduction of the nickel ions occur, as revealed here by an *in situ* TEM study allowing the recording of images of a selected zone of the sample while being heated.

Acknowledgements

References

1 F. Fajula, D. Plee, *Stud. Surf. Sci. Catal.*, 1994, **85**, 633.
2 F. Di Renzo, F. Fajula, Stud. Surf. Sci. Catal., 2005, **157**, 1.
3 N.S. Nesterenko, A.S. Kuznetsov, S.E. Timoshin, F. Fajula, I. Ivanova, Appl. Catal., A: General, 2006, **307**(1), 70.
4 A.N. Mlinar, G.B. Baur, G.G. Bong, A. Getsoian, A.T. Bell, Alexis T., J. Catal., 2012, **296**, 156.
5 A. Goursot, B. Coq, F. Fajula, J. Catal., 2003, **216**(1-2), 324.
6 D.W. Breck, E. M. Flanigen, Mol. Sieves, Pap. Conf., 1968, 47.
7 R.M. Barrer, R.P. Townsend, J. Chem. Soc., Farad. Trans. 2, 1984, **80**(5), 629.
8 W.J. Mortie, E. Van den Bossche, J.B. Uytterhoeve, Zeolites, 1984, **4**(1), 41.
9 G. Delahay, E.A. Villagomez, J.-M. Ducere, D. Berthomieu, A. Goursot, B. Coq, ChemPhysChem, 2002, **3**(8), 686.
10 D. Berthomieu, G. Delahay, Catal. Rev. Sci. Eng., 2006, **48**, 269.
11 A. Goursot, B. Coq, F. Fajula, J. Catal., 2003, **216**(1-2), 324.
12 Ch. Baerlocher, L.B. McCusker, D.H. Olson, Atlas of Zeolite Framework Types, 6th revised edition, Elsevier, Amsterdam, 2007.
13 T. Frising P. Leflaive, Microporous Mesoporous Mater., 2008, **114**(1-3), 27.
14 W.J. Mortier, Compilation of Extra-framework Sites in Zeolites, Butterworths, Guildford, 1982, RI98.
15 Guesmi, D. Costa, D. Berthomieu, P. Massiani, J. Phys. Chem. C, 2011, **115**(13), 5607.
16 H. Guesmi, P. Massiani, Catal. Today, 2011, **177**, 25.
17 M.Jeffroy, E. Borissenko, A. Boutin, A.Di Lella, F.Porcher, M. Souhassou, C. Lecomte, A.H. Fuchs, Microporous Mesoporous Mater., 2011, **138,** 45.
18 W. Louisfrema, B. Rotenberg, F. Porcher, J.L. Paillaud, P. Massiani, A. Boutin, Mol. Simul., 2015, **41**(16-17), 1371.
19 D.H. Olson, J. Phys. Chem., 1968, **72**, 4366.
20 Y. Horikawa, N. Ohnishi, K. Hiraga, Mater. Sci. Eng., 1996, **A217/218**, 139.
21 Y. Sendoda, Y. Ono, T. Keii, J. Catal. 1975, **39**, 357.
22 J.F. Groust, C. Pommier, L. Stievano, F. Villain, C. Giorgetti, F. Baudelet, P. Massiani, Catal. Lett., 2005, **102**, 257.
23 J.M. Thomas, C. Williams, T. Rayment, J. Chem. Soc., Faraday Trans. 1, 1988, **84**, 2915.
24 E. Doorhyhee, C.R. Catlow, J.W. Couves, P.J. Maddox, J.M. Thomas, G.N. Greaves, A.T. Steel, R.P. Townsend, J. Phys. Chem., 1991, 95, 4514.
25 N.D. Hutson, B. A. Reisner, R. T. Yang, B.H. Toby, Chem. Mater., 2000, **12**, 3020.
26 A.J. Fowkes, R.M. Ibberson, M.J. Rosseinsky, Chem. Mater., 2002, **14**(2), 590.
27 C. Forano, R.C.T. Slade, E. Krogh Andersen, I.G. Krogh Andersen, E. Prince, J. Solid State Chem., 1989, **82**, 95.
28 J. Plevert, F. Di Renzo, F. Fajula, G. Chiari, J. Phys. Chem. B, 1997, **101**, 10340.
29 J. Plevert, F. Di Renzo, F. Fajula, G. Chiari, Proceed. 12th Int. Zeol. Conf., Baltimore, 1998, **1**, 135.
30 V. Bosacek, S. Beran, Z. Jirak, J. Phys. Chem. 1981, **85**, 3856.
31 J.M. Adams, L.V.C. Rees, J. Solid State Chem., 1986, **62**, 184.
32 J. Hunger, I.A. Beta, H. Bohlig, C. Ling, H. Jobic, B. Hunger, J. Phys. Chem. B, 2006, **110**, 342.
33 A. Martucci, G. Cruciani, A. Alberti, C. Ritter, P. Ciambelli, M. Rapacciuolo, Microporous Mesoporous Mater., 2000, **35–36**, 405.
34 M. Czjzek, H. Jobic, A.N. Fitch, T. Vogt, J. Phys. Chem., 1992, **96**(4), 1535.
35 R.M. Haniffa, K. Seff, J. Phys. Chem. B, 1998, **102**, 2688.
36 G. Vitale, C. F. Mellot, A. K. Cheetham, J. Phys. Chem. B, 1997, **101**, 9887.
37 M. Kuronen, M. Weller, R. Townsend, R. Harjula, Reactive & Functional Polymers, 2006, 66, 1350.
38 A. Wozniak, B. Marler, K. Angermund, H. Gies, Chem. Mater., 2008, **20**, 5968.
39 A.N. Fitch, H. Jobic and A. Renouprez, J. Phys. Chem., 1986, **90**, 1311.
40 Intern. Tables for Crystallography, Vol. C, Third Edition, p446.
41 Rietveld, H. M. J. Appl. Crystallogr. 1969, **2**, 65–71.
42 J. Rodriguez-Carvajal, Physica B, 1993, **192**, 55; J Rodríguez-Carvajal, Commission on powder diffraction (IUCr). Newsletter 26, 12.
43 M.M.J. Treacy, J.B. Higgins (Eds.) in "*Collection of Simulated XRD Powder Patterns for Zeolites",* fourth revision, 2001.
44 M.P. Attfield, A.W. Sleight, Chem. Commun., 1998, 601.
45 A.N. Christensen, M.S. Lehmann, J. Pannetier, J. Appl. Crystallogr., 1985, **18**, 170.
46 W. Abriel, K. Reisdorf, J. Pannetier, J. Solid State Chem., 1990, **85**, 23.
47 J.W. Couves, R.H. Jones, J. M. Thomas, Adv. Mater., 1990, **2**(4), 181.

The incoherent signal in neutron diffraction patterns allows correlating in real time hydration-dehydration levels and structural changes in zeolites.